Phosphorus recovery from municipal sludge-derived hydrochar: Insights into leaching mechanisms and hydroxyapatite synthesis

Huan Liu, Nathalie Lyczko, Ange Nzihou, Cigdem Eskicioglu

Phosphorus recovery from municipal sludge-derived hydrochar: Insights into leaching mechanisms and hydroxyapatite synthesis

Huan Liu [a], Nathalie Lyczko [b], Ange Nzihou [b,c,d], Cigdem Eskicioglu [a,*]

[a] UBC Bioreactor Technology Group, School of Engineering, The University of British Columbia, Okanagan Campus, 1137 Alumni Avenue, Kelowna, British Columbia V1V 1V7, Canada

[b] Université de Toulouse, IMT Mines Albi, RAPSODEE CNRS UMR 5302, Campus Jarlard, F.81013 Albi Cedex 09, France

[c] Princeton University, School of Engineering and Applied Science, Princeton, NJ 08544, United States

[d] Princeton University, Andlinger Center for Energy and the Environment, Princeton, NJ 08544, United States

Hydrothermal liquefaction has the potential to exploit resources from municipal sewage sludge. It converts most organics into a liquid biofuel (biocrude), concentrates P in the solid residue (hydrochar), and consequently enables its efficient recovery. This study thoroughly evaluated the effects of extraction conditions on P and metal release from hydrochar by nitric acid. Among assessed factors, acid normality (0.02–1 N), liquid-to-solid ratio (5–100 mL/g), and contact time (0–24 h) had positive effects while decreasing eluate pH (0.5–4) improved leaching efficiencies of P and metals. Notably, eluate pH played a dominant role in P leaching and pH < 1.5 was crucial for complete extraction. P and metal leaching from hydrochar have strong interactions and their leaching mechanism was identified as product layer diffusion using the shrinking core model. This suggests that the leaching efficiency is susceptible to agitation and particle size but not temperature. Using 10 mL/g of 0.6 N HNO_3 for 2 h was considered the best extraction condition for efficient P leaching (nearly 100%) and minimization of cost and contaminants (heavy metals). Following extraction, adding $Ca(OH)_2$ at a Ca:P molar ratio of 1.7–2 precipitated most P (99–100%) at pH 5–6, while a higher pH (13) synthesized hydroxyapatite. The recovered precipitates had high plant availability (61–100%) of P and satisfactory concentrations of heavy metals as fertilizers in Canada and the US. Overall, this study established reproducible procedures for P recovery from hydrochar and advanced one step closer to wastewater biorefinery.

1. Introduction

Phosphorus (P) is a life-essential nutrient element that has been listed as a critical raw material in many countries (e.g., EU). It is a non-renewable and non-substitutable resource. However, its source, phosphate rock reserves, is only located in a few countries, such as Morocco and Western Sahara (72% of the world reserve) (Liu et al., 2021b). Many countries partially or entirely depend on imports of P resources and products. The uneven distribution of phosphate rock has created polit-ical and economic risks. On the other hand, P discharge from waste sources, such as wastewater, is a major contributor to aquatic eutrophication, causing severe environmental challenges (Huang et al., 2017). Therefore, P recovery from P-rich residues and its valorization provide a double benefit – a geographically distributed secondary P source and environmental conservation.

Municipal sludge generated from wastewater treatment plants (WWTPs) has gained much attention as a promising P source. It is attractive for high levels of P (1–3.8% on a dry basis, db), large quantities (>45 million dry tonnes/year), and readily available (Liu et al., 2021a, 2021b). Raw sludge contains high moisture (up to 98%) and its solids generally consist of 40–70%, db of volatile matter and 20–50%, db of ash, including some contaminants, such as pathogens, organic

Abbreviations: AMs, Alkali Metals; AEMs, Alkaline Earth Metals; AP, Apatite Phosphorus; FTIR, Fourier Transform Infrared Spectroscopy; HHV, Higher Heating Value; HTL, Hydrothermal Liquefaction; ISSA, Incinerated Sewage Sludge Ash; ICP-OES, Inductively Coupled Plasma Optical Emission Spectroscopy; IP, Inorganic Phosphorus; L/S, Liquid-to-Solid Ratio; NAIP, Non-Apatite Inorganic Phosphorus; OP, Organic Phosphorus; PPE, Phosphorus Precipitation Efficiency; PRE, Phosphorus Recovery Efficiency; PTMs, Post-Transition Metals; PC, Principal Component; PCA, Principal Component Analysis; SI, Saturation Index; TP, Total Phosphorus; TMs, Transition Metals; WWTPs, Wastewater Treatment Plants; XRD, X-Ray Diffraction.

pollutants, heavy metals, and micropollutants (Liu et al., 2021a). A promising technology, hydrothermal liquefaction (HTL), could promote nutrient recovery by converting the organic fraction into a liquid biofuel (called biocrude) and concentrating P in the solid residue (named hydrochar) (Shi et al., 2019). Using water as the reaction medium, HTL is particularly suitable for treating sludge and tackling its high moisture and low dewaterability (Basar et al., 2021). HTL is typically performed at a closed subcritical condition (280–374 °C and 8–22 MPa) that is milder than other thermochemical processes, e.g., pyrolysis, gasifica-tion, and incineration. After reaction, organic matter is mostly trans-formed into petroleum-like biocrude and some are dissolved in the process water (called HTL aqueous), whereas minor carbonaceous ma-terial with most minerals is retained in hydrochar (Basar et al., 2023; Liu et al., 2022). Consequently, the dry-weight P concentration in hydrochar is around five times higher than that of feedstock sludge, reaching up to 10% (Ovsyannikova et al., 2020). This makes hydrochar comparable to low-grade phosphate rock (around 8% P) (Fahimi et al., 2021). However, reusing hydrochar as a fertilizer is restricted for the excess content of accumulated heavy metals (Liu et al., 2023). There-fore, P recovery represents an important state for resource sustainability and circular economy.

In recent years, much attention has been given to the fate and transformation of P during hydrothermal treatment (Huang et al., 2017; Shi et al., 2019; Wang et al., 2020). It is generally agreed that >80% P from sludge is captured in hydrochar and major metals (e.g., Al, Ca, and Fe) strongly affect P speciation and the subsequent recovery process. Standing on the experience of incinerated sewage sludge ash, wet-chemical extraction and precipitation have been identified as the most suitable approach for P recovery due to their cost-effectiveness and environmental sustainability (Fahimi et al., 2021; Liu et al., 2021b). To date, a few studies attempted to recover P from hydrochar using various extractants, including inorganic acids (H_2SO_4 and HCl) (Ovsyannikova et al., 2020; Pérez et al., 2021), organic acids (citric and oxalic acid) (Becker et al., 2019; Ovsyannikova et al., 2020; Pérez et al., 2022), and bases (NaOH and KOH) (Li et al., 2020; Ovsyannikova et al., 2020, 2019). Acidic leaching is commonly used for its high efficiency. High-temperature HTL typically transforms Al/Fe-bound phosphate into Ca-phosphate, thus limiting the efficiency (<70%) of alkaline leaching (Liu et al., 2021b). Besides, acidic leaching can remove ash contents and thus enhance the reuse value of hydrochar residue as a solid fuel (Marin-Batista et al., 2020). The reported extractants also have their limitations: Sulfuric acid is cheap but the process generates a large amount of gypsum and limits the reusability of hydrochar; hydrochloric acid is efficient but corrosive and scarcely used industrially; organic acids are too costly for industrial application; bases are only applicable to Al/Fe-bound phosphate (Li et al., 2020; Soltani et al., 2019). Extraction is the critical step for P recovery, but optimizing extraction conditions, such as liquid-to-solid (L/S) ratio, extractant concentration, leaching time, and pH, is rarely reported. The leaching mechanisms of P and co-leached metals from hydrochar are lacking.

In addition, few studies investigated the precipitation of P from extract as interesting products. Struvite ($MgNH_4PO_4{\cdot}6H_2O$) and K-struvite ($MgKPO_4{\cdot}6H_2O$) were recovered previously but they require expensive chemical input (e.g., $MgCl_2$) and face challenges of achieving the optimal stoichiometric ratio between the necessary elements (Becker et al., 2019; Li et al., 2020; Ovsyannikova et al., 2020). There-fore, more robust P recovery processes for hydrochar should be devel-oped to realize industrialization. Hydroxyapatite is a unique material for its wide application in agriculture, biomedicine, environmental reme-diation, catalysis, and energy storage (Pham Minh et al., 2014). It has relatively good sell values and requires cheap chemical input (such as lime) for production (Liu et al., 2021b). However, the current studies about hydroxyapatite synthesis are limited to pure chemicals or sources with trace foreign elements (Agbeboh et al., 2020; Arokiasamy et al., 2022). Recovering P as hydroxyapatite from complex waste streams such as hydrochar is rarely reported and may face some challenges, thus requiring attention.

Recognizing the benefits of incorporating HTL into WWTPs (Liu et al., 2022) and the promise of P recovery from hydrochar (Liu et al., 2023), this study aims at developing suitable P recovery procedures for sludge-derived hydrochar by wet chemical extraction and precipitation. Nitric acid was selected as the extractant for the following reasons: Efficient, inexpensive, widely used in industry, no gypsum generation, recoverable, and recyclable (Banihashemi et al., 2019). Firstly, the ef-fects of various extraction conditions on the leaching of P and metals were assessed on hydrochar from one HTL condition. The interactions between P and metals were explained. Secondly, the leaching kinetics and mechanisms were identified for the first time to assist the process optimization. Thirdly, the challenges and insights of synthesizing hy-droxyapatite from hydrochar leachate were unrevealed. In particular, the compositions of recovered products were examined using various techniques (e.g., inductively coupled plasma, Fourier transform infrared spectroscopy and X-ray diffraction) to produce qualified fertilizers. Ul-timately, the applicability of established P recovery procedures was validated by applying it to hydrochar samples obtained at different HTL conditions (temperatures/pressures). The results are important for wastewater utilities aiming to develop a robust HTL process in tandem with P recovery with a clear/safe ultimate disposal route for all product streams.

2. Materials and methods

2.1. Materials

Municipal mixed (primary and secondary) sludge (Table S1) was obtained from a local WWTP in BC, Canada. The WWTP has primary and two-stage secondary (biological) treatment processes including trickling filters followed by solid-contact tanks. The mixed sludge was dewatered to 20% solids content through centrifugation. Hydrochar (HC350) was produced from the dewatered sludge at an HTL reaction temperature of 350 °C for a residence time of 15 min (a commonly reported condition) (Marrone et al., 2018; Ovsyannikova et al., 2020). After reaction, HTL aqueous was separated by centrifugation (4000 × g for 15 min) and filtration (20 μm) from biocrude and hydrochar. Hydrochar was extracted from biocrude by washing with 1-L dichloromethane. Fol-lowed by drying (105 °C for 24 h) and homogenizing by mortar grinding, hydrochar was stored at 4 °C for analysis. Detailed HTL pro-cedures can be found in a previous report (Liu et al., 2022). Deionized Type I water (resistivity ≥ 18.2 MΩ·cm) was used for preparing all re-agents. The characterization of hydrochar has been previously reported, including proximate and ultimate analysis, higher heating value (HHV), particle size distribution, total P (TP) and metals, P species (organic P – OP, inorganic P – IP, apatite P – AP, and non-apatite IP – NAIP), Fourier transform infrared spectroscopy (FTIR), and X-ray diffraction (XRD) analysis (Liu et al., 2023).

2.2. Leaching procedures

The extraction efficiencies of P and metals by HNO_3 solutions were assessed to evaluate the effects of L/S ratio (5–100 mL/g), acid normality (0.02–1 N), and contact time (0–24 h). In each experiment, 20 mL of extractant solutions with hydrochar samples were transferred into 30 mL polyethylene tubes. The tubes were sealed and well shaken by an end-over-end rotator (GFL 3040) at 20 ± 1 rpm and room temperature (20 ± 2 °C). After extraction and syringe filtration (0.45 μm), P and metal contents in extracts were quantified by an inductively coupled plasma optical emission spectroscopy (ICP-OES, Jobin Yvon Horiba ULTIMA 2). The pH of the eluate was measured immediately. The leaching efficiency (η,%) of P and metals can be calculated by dividing the total as shown in Eq. (S1) (see supplementary material). All extraction experiments were completed at least in duplicates. In each test, two experimental blanks were performed on extractants in empty

tubes.

2.3. Leaching kinetics

After determining extracted P and metals, the shrinking core model (for constant particle size), most commonly used in the literature, was employed to identify the leaching mechanisms (Faraji et al., 2020). It describes a solid-liquid process in which leaching agents diffuse through the liquid film around the particle and solid product layer and react on the unreacted core surface. However, this model assumes that the shape and size of solid particles remain unchanged during the leaching pro-cess; the effective diffusivity is constant; and the reaction is first-order and irreversible (Liddell, 2005). The leaching agent should be exces-sive so that its concentration is constant, which generally applies at a high L/S ratio. The following rate-limiting steps can be identified during the leaching process and expressed by the apparent rate equations:

$$\text{Liquid film diffusion}: \ X = \frac{1}{\tau_F} t \tag{1}$$

$$\text{Product layer diffusion}: \ 1 - 3(1-X)^{2/3} + 2(1-X) = \frac{1}{\tau_P} t \tag{2}$$

$$\text{Chemical reaction}: \ 1 - (1-X)^{1/3} = \frac{1}{\tau_R} t \tag{3}$$

where X (=η/100) is the conversion or ion leaching rate (0–1) at the leaching time t (min); τ_F, τ_P, and τ_R are the completion time (min) of each leaching step.

To determine which step controls the leaching rate (significantly slower than the others), the conversion side (left) of each equation versus time was plotted to obtain the best linear relationship by comparing their coefficients of determination (R^2). All linear fitting must fix the intercept at 0 (i.e., 0 conversion at 0 time) for a correct evaluation.

In some cases, the rate-limiting step cannot be clearly defined using a single mechanism or more than one step may control the rate simulta-neously. The following equation combining all three mechanisms was developed to estimate the time constants (Nazemi et al., 2011).

$$t = \tau_F \mathrm{X} + \tau_P \left[1 - 3(1-\mathrm{X})^{2/3} + 2(1-\mathrm{X})\right] + \tau_R \left[1 - (1-\mathrm{X})^{1/3}\right] \tag{4}$$

The constants in Eq. (4) can be calculated through a constrained least square optimization by minimizing φ (subject to τ_F, τ_P, and $\tau_R \geq 0$) in the below equation using MATLAB.

$$\varphi = \sum_i \left\{ \tau_F X_i + \tau_P \left[1 - 3(1-X_i)^{\frac{2}{3}} + 2(1-X_i)\right] + \tau_R \left[1 - (1-X_i)^{\frac{1}{3}}\right] - t_i \right\}^2 \tag{5}$$

where i is the number of data points.

2.4. Precipitation as hydroxyapatite

By dosing $Ca(OH)_2$ to acidic P extracts and controlling the Ca:P molar ratio at around 1.67 (Eq. (6)), hydroxyapatite could be synthe-sized (Verwilghen et al., 2007).

$$10Ca(OH)_2 \ + \ 6H_3PO_4 \rightarrow Ca_{10}(PO_4)_6(OH)_2 \ + \ 18H_2O \tag{6}$$

Calcium hydroxide (98%, KFN nekablanc®0) was suspended in Type I water to form a lime solution (30 g/L). P extracts were dosed dropwise to a pre-determined amount of lime solutions based on Ca:P ratios. The designated pH was achieved by injecting 2 M KOH solutions. After stirring at 300 rpm for 24 h at room temperature for maturation, the mixture was centrifugated at 3000 × g for 5 min, and the supernatant was sampled and filtered through 0.45 μm syringe filters for the elemental analysis by ICP-OES. The precipitate was collected by vacuum filtration (0.45 μm), washed with 1 L Type I water, dried at 105 °C for 24 h, and stored at 4 °C before analysis (named HAP-pH). The P precipi-tation efficiency (PPE,%) and overall P recovery efficiency (PRE,%) were calculated using Eqs. (S2) and (S3).

Table 1
Characteristics of hydrochar (dry basis).

Parameters[a]	Values	Total inorganics	Concentrations (mg/kg, n = 3)
Ultimate analysis (n = 2)		**Alkali metals**	
C (%)	28.7 ± 0.3	Na	1076±113
H (%)	2.2 ± 0.1	K	2342±223
N (%)	2.9 ± 0.1	**Alkaline earth metals**	
S (%)	0.5 ± 0.1	Ba	742±64
O (%)	7.9 ± 0.5	Ca	44526±5616
Proximate analysis (n = 2)		Mg	6589±511
Ash (%)	57.8 ± 0.2	**Transition metals**	
Volatile matter (%)	26.39 ±0.01	Cd	7 ± 1
Fixed carbon (%)	15.8 ± 0.1	Cr	143±20
Fuel ratio (–)	0.60±0.01	Co	8 ± 1
HHV (MJ/kg)	12.2 ± 0.2	Cu	1589±154
P species (n = 3)		Fe	87116±1824
OP (mg/g)	0.28±0.02	Mn	741±84
IP (mg/g)	54±1	Mo	42±7
NAIP (mg/g)	29.8 ± 0.6	Hg	2.5 ± 0.7
AP (mg/g)	24.1 ± 0.6	Ni	130±15
TP (mg/g)	57±6	Ag	8 ± 1
		V	28±4
		Zn	2762±257
		Post-transition metals	
		Al	13375±661
		Pb	109±14
		Non-metals	
		As	4.4 ± 0.5
		Se	10±1

[a] HHV = higher heating value; OP = organic phosphorus; IP = inorganic phosphorus; NAIP = non-apatite IP; AP = apatite phosphorus; TP = total phosphorus.

2.5. Characterization of recovered precipitates

The recovered P products were pulverized for XRD and FTIR analysis. The total elemental concentrations were measured by ICP-OES after block digestion in aqua regia at 90 °C for 1 h (Rego de Vasconcelos et al., 2018). The plant-available P was estimated by 2% citric acid (20 g/L) following EN 15,920:2011. Briefly, 0.2 g samples were extracted at an L/S of 100 mL/g using end-over-end rotation (20 ± 1 rpm) for 30 min at room temperature. Followed by immediate filtration (0.45 μm syringe filters), the extractable P was determined by ICP-OES.

2.6. Application of optimal recovery procedures

At a different time, mixed sludge was obtained from the same WWTP. The sludge was dewatered to 20% solids content and processed at HTL temperatures of 290, 325, and 360 °C (15 min residence time) to pro-duce different hydrochars of HC290, HC325, and HC360, respectively (Liu et al., 2023). The optimal extraction and precipitation conditions were applied to those different hydrochar samples to validate the P re-covery procedures.

3. Results and discussion

3.1. Hydrochar composition

The composition of hydrochar (HC350) is shown in Table 1. Hydrochar had a high ash content, 57.8% on a dry basis (db), with inorganic contents ranked as transition metals (TMs) > P > alkaline earth metals (AEMs) > post-transition metals (PTMs) > alkali metals (AMs). Due to the major presence of Fe, hydrochar showed a high

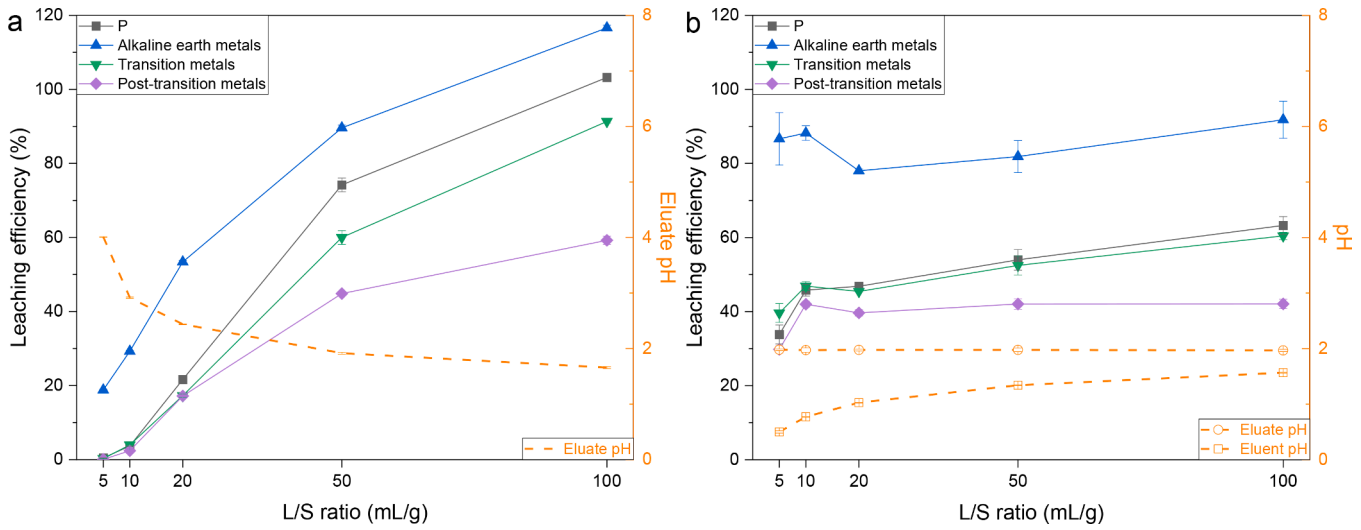

Fig. 1. Effects of L/S ratio on P and metal release at (a) 0.1 N HNO_3 and (b) fixed eluate pH 2. Leaching time: 24 h.

portion of NAIP (55% relative to TP), while the great amount of Ca-bound AP indicated that acidic extraction would be more feasible than alkalic extraction for efficient P recovery. Hydrochar also contained excessive amounts of heavy metals (e.g., Mo and Zn), raising concerns for direct land application. Therefore, P recovery for separating from heavy metals is necessary. The XRD patterns (Fig. S1) suggest that the major crystal phases in hydrochar were cordierite ($Mg_{6.5}FeAl_{15.5}Si_{19.3}O_{76.9}$), diopside ($Ca_4Mg_{3.6}Fe_{0.8}Si_{7.6}O_{24}$), and enstatite ($Al_{0.2}Fe_{1.2}Mg_{14.6}Si_{15.8}O_{48}$), as agreed to previous studies (Liu et al., 2021b).

3.2. Leaching tests

For the evaluation of leaching behavior and extraction efficiency of P and metals, the effects of L/S ratio, nitric acid concentration, and leaching time were examined. Selected metals were presented in groups or families that are expected to have close behavior, including AEMs (Ca and Mg), TMs (Fe, Zn, Cu, Mn, Cr, Ni, and Mo), and PTMs (Al and Pb). Those metals typically have strong affinities with phosphate.

3.2.1. Effect of L/S ratio

As shown in Fig. 1a, at constant acid normality (0.1 N) and leaching time (24 h), the release of P and metals significantly enhanced with increasing L/S ratio (5–100 mL/g), while the eluate pH at the end of extraction decreased dramatically from 4 to <2. They all showed limited extraction (<20%) at a low L/S (5 mL/g). Notably, the leaching effi-ciency of AEMs was much higher than P, TMs, and PTMs, and P and AEMs reached nearly 100% extraction at 100 mL/g (final pH around 1.6). Over 100% extraction was considered errors from inhomogeneous samples, underestimated total, and high dilution factors for analysis.

When fixing the eluate pH at 2, the L/S ratio showed limited impacts on leaching efficiencies compared to fixed acid concentration (Fig. 1b). The leaching of AEMs remained above 80%, whereas the sharp rise of other metals only occurred from 5 to 10 mL/g, with limited increase afterward. This indicated that constraining final pH could strongly hinder the release of P, TMs, and PTMs. At 10–100 mL/g, P and TMs showed nearly the same leaching behaviors, suggesting P was mainly released from compounds bound to TMs (e.g., iron phosphates). How-ever, the P extraction at 100 mL/g was still <60%, suggesting a lower pH is necessary for efficient P recovery.

At both fixed acid concentration and eluate pH, the overall release followed the order of AEMs > *P* > TMs > PTMs, implying that P leaching efficiency was probably regulated by TMs and PTMs. Analysis of vari-ance showed that L/S ratio had a significant effect ($p = 0.007$) on P release, while eluate pH exhibited a much higher impact ($p < 0.0001$).

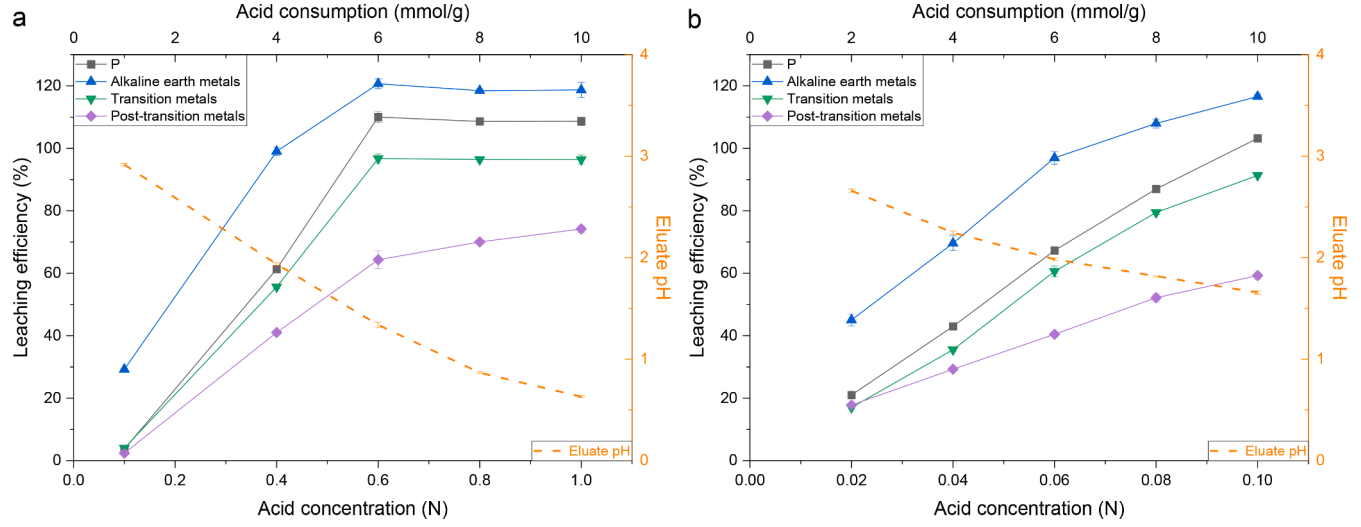

Fig. 2. Effects of acid normality on P and metal release at an L/S of (a) 10 mL/g and (b) 100 mL/g. Leaching time: 24 h.

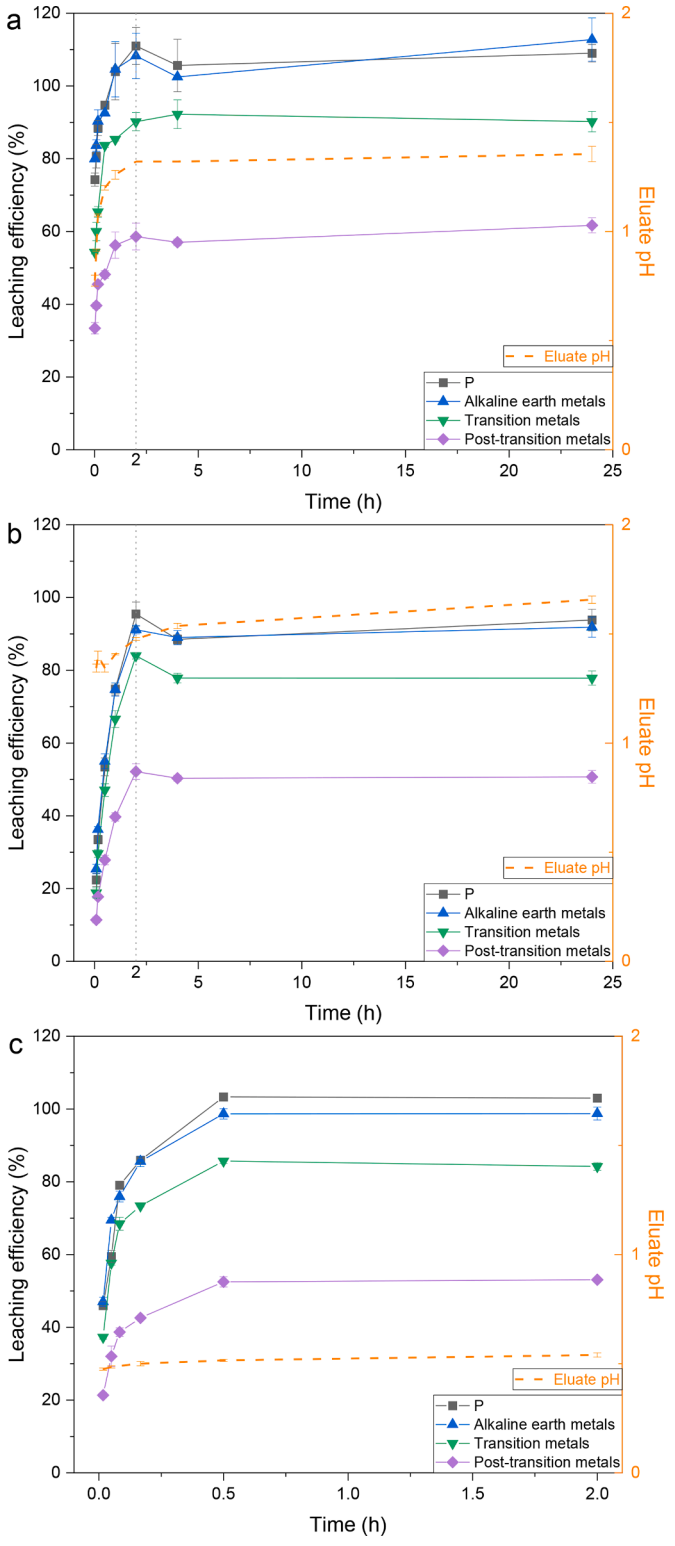

Fig. 3. Effects of leaching time on P and metal release at (a) L/S = 10 mL/g (0.6 N HNO_3), (b) L/S = 100 mL/g (0.1 N HNO_3), and (c) L/S = 100 mL/g (0.6 N HNO_3).

3.2.2. *Effect of acid concentration*

The leaching of P and metals at different acid concentrations was investigated at 10 and 100 mL/g for 24 h. At 10 mL/g, the leaching of P and metals increased sharply by increasing acid concentration from 0.1 N to 0.6 N for more free H^+ (Fig. 2a). Above 0.6 N (eluate pH < 1.4), P, AEMs, and TMs reached the plateau or maximum, while PTMs continued leaching but the rate decreased. Another study also found that the leaching of P and metals from primary sludge-derived hydrochar reached equilibrium at 0.4–1 N of sulfuric acid with an L/S of 10 mL/g (Ovsyannikova et al., 2020). Similarly, at 100 mL/g (Fig. 2b), the extraction efficiency of P and each metal group enhanced constantly by increasing acid normality from 0.02 N to 0.1 N for maximum leaching. However, the plateau region was not observed at 0.02–0.1 N. For cost-effectiveness, 0.6 N and 0.1 N were considered the most suitable condition for P leaching at the L/S of 10 and 100 mL/g, respectively.

When normalizing the acid consumption per sample amount as calculated by Eq. (7), there was a substantial difference between the two L/S ratios (Fig. 2). At the same acid consumption, the leaching efficiency of P and metals were much higher at 10 mL/g than those at 100 mL/g. The difference was attributed to the elevated pH by dilution factor × 10 at the higher L/S. To achieve complete leaching of P, 6 and 10 mmol of nitric acid per g of sample were needed at the L/S of 10 and 100 mL/g, respectively. Therefore, a lower L/S ratio was more efficient and economical for P extraction.

$$Acid\ consumption\ (mmol/g) = Acid\ concentration\ (mol/L) \times L/S\ (mL/g) \quad (7)$$

3.2.3. *Effect of leaching time*

The influence of leaching time was evaluated at various L/S ratios and HNO_3 concentrations. Fig. 3 illustrates that the extraction of each element increased with leaching time and eventually achieved equilibrium within 2 h under both leaching conditions. With the release of P and metals, the eluate pH of leachate also increased and gradually reached a plateau. At 10 mL/g (0.6 N HNO_3), almost all P and AEMs and nearly 90% of TMs and 60% of PTMs were released at 2 h (Fig. 3a). Under 100 mL/g (0.1 N HNO_3), >90% of P and AEMs, >80% of TMs, and around 50% of PTMs were extracted in 2 h (Fig. 3b). Using H_2SO_4, HCl, and citric acid, a few studies found the maximum P extraction from sludge-derived hydrochar could be achieved within 2 h (Becker et al., 2019; Ovsyannikova et al., 2020). Most studies confirmed that 2 h is sufficient to leach most P from incinerated sewage sludge ash (ISSA) (Liu et al., 2021b). However, using excessive acid (0.6 N HNO_3) and a high L/S ratio (100 mL/g) significantly accelerated the leaching process to complete within 0.5 h (Fig. 3c). Notably, the initial leaching rate was much faster at a higher L/S ratio or stronger acid normality under identical conditions, which was probably linked to the lower pH. Notably, leaching efficiencies of P and metal decreased after 2 h in Fig. 3a and b, indicating adsorption or reprecipitation of metal phos-phates during long-term extraction (Ottosen et al., 2013). Therefore, 2 h was considered the optimal leaching time. Nevertheless, there is a compromise between complete leaching time and acid amount.

3.2.4. *Dependency on pH*

The leaching efficiency of P was found to depend on the eluate pH at the end of extraction Fig. 4a). The fitting analysis suggested a logistic curve of P release in terms of eluate pH (adjusted $R^2 = 0.99$, $p < 0.05$) regardless of the L/S ratio at a leaching time of 24 h. The P leaching efficiency was nearly 0 at a final pH > 3, which improved sharply following an "S" curve with decreased pH until reaching the complete extraction at a pH < 1.5. This finding agrees with a previous literature review which summarized that pH < 2 is necessary to extract most P from sludge-derived ash and hydrochar (Liu et al., 2021b). Based on the eluate pH, the reactions during leaching can be generalized into two steps shown by Eq. (8) and Eqs. (9)–((11), respectively Liu et al., 2021b), which can be explained by the solubility product constant (K_{sp}) and calculated molar solubility (s) of phosphates. Although AP and NAIP have low K_{sp} values and thus low solubilities, they could dissolve in sufficient acid since a little soluble PO_4^{3-} would protonate and form hydrogen phosphates and eventually phosphoric acid (Eqs. (12)–(14) (Luyckx et al., 2020), which promotes the dissolution based on the Le Chatelier's principle. At a less acidic pH of 2–3, mainly calcium

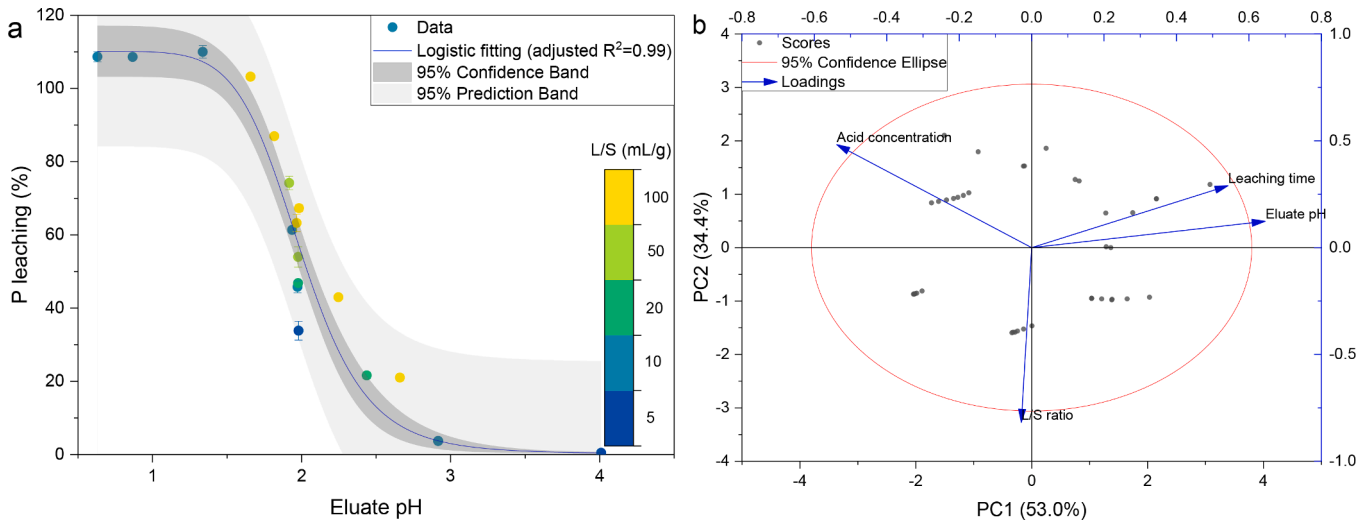

Fig. 4. (a) P leaching efficiency as a function of eluate pH (leaching time 24 h) and (b) principal component analysis (PCA) biplot of leaching factors regarding P release based on correlation matrix.

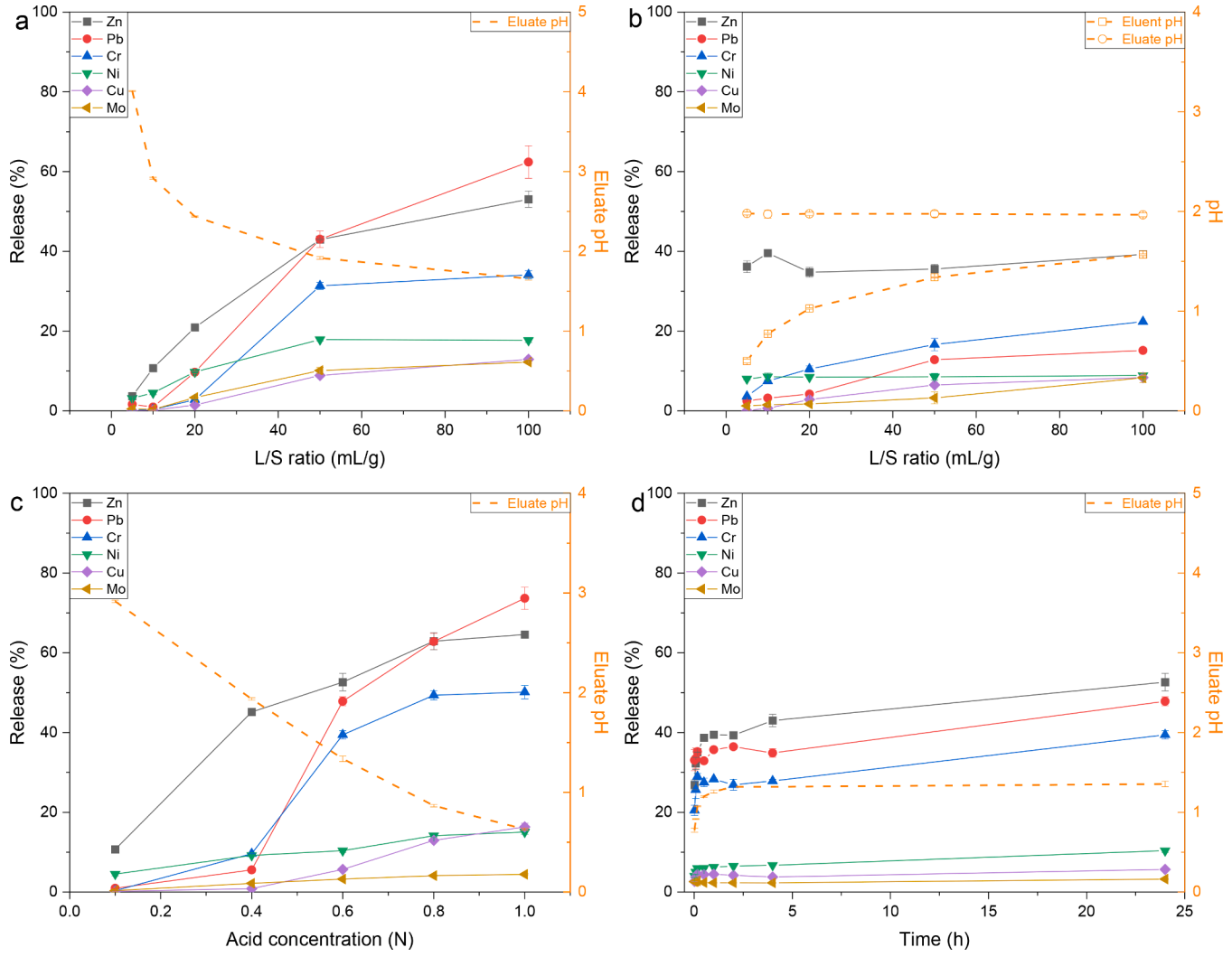

Fig. 5. The release of heavy metals in terms of (a) L/S ratio – fixed 0.1 N HNO_3 for 24 h, (b) L/S ratio – fixed eluate pH at 2 for 24 h, (c) acid concentration (10 mL/g for 24 h), and (d) leaching time (10 mL/g and 0.6 N HNO_3).

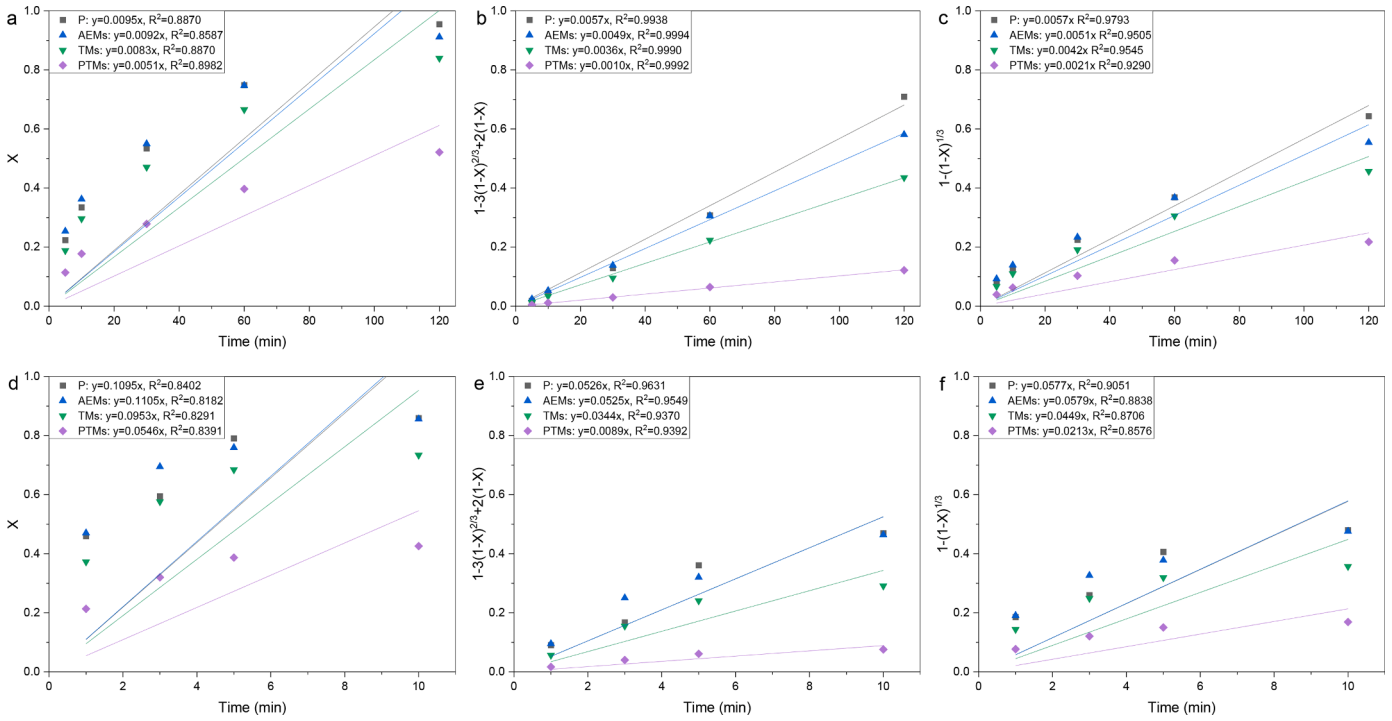

Fig. 6. Leaching data fitted to controlling mechanisms of liquid film diffusion, product layer diffusion, and chemical reaction in 100 mL/g of 0.1 N (a–c) and 0.6 N (d–f) HNO_3.

phosphates (Ca-P) dissolve as they have a higher molar solubility, while aluminum (Al-P) and iron phosphates (Fe-P) only partially dissolve (He et al., 2020). For pH < 2, more ferrous, aluminum and ferric phosphates could solubilize, and P leaching efficiency enhanced steeply until fully soluble by enough acid. This is in line with a previous study that most P was released from $AlPO_4$ at pH = 1 (Toor and Kim, 2019). Over 55% of NAIP in hydrochar suggested that only an eluate pH < 1.5 could achieve the full extraction of P. The XRD analysis of hydrochar residue after leaching (Fig. S1a) confirmed that high-intensity Al and Fe minerals, e. g., cordierite and diopside, were remaining at final pH around 2–3 (LS10–0.1 N and LS10–0.4 N), which disappeared at eluate pH < 1.5 (LS10–0.6 N). The FTIR spectra (Fig. S1b) implied that phosphates (band at 1000–1100 cm^{-1}) greatly leached and disappeared from hydrochar with decreased pH (increased acid concentration), while iron oxides (bands at 550 and 460 cm^{-1}) did not change much until using 0.6 N HNO_3. Both XRD (ilvaite peaks) and FTIR (band 460 cm^{-1}) results indicated some acid-insoluble Fe/Al silicates were retained in leached hydrochar.

- $2 \leq pH < 3$ (25 °C):

$$Ca_3(PO_4)_2 \rightleftharpoons 3Ca^{2+} + 2PO_4^{3-},\ K_{sp} = 2.1 \times 10^{-33},\ s = 1.1 \times 10^{-7} M \quad (8)$$

- pH < 2 (25 °C):

$$Fe_3(PO_4)_2 \rightleftharpoons 3Fe^{2+} + 2PO_4^{3-}, K_{sp} = 1.6 \times 10^{-36},\ s = 2.7 \times 10^{-8} M \quad (9)$$

$$AlPO_4 \rightleftharpoons Al^{3+} + PO_4^{3-},\ K_{sp} = 9.8 \times 10^{-21},\ s = 9.9 \times 10^{-11} M \quad (10)$$

$$FePO_4 \rightleftharpoons Fe^{3+} + PO_4^{3-},\ K_{sp} = 1.3 \times 10^{-22},\ s = 1.1 \times 10^{-11} M \quad (11)$$

- pH < 3 (25 °C):

$$PO_4^{3-} + H^+ \rightleftharpoons HPO_4^{2-},\ pK_a = 12.32 \quad (12)$$

$$HPO_4^{2-} + H^+ \rightleftharpoons H_2PO_4^-,\ pK_a = 7.21 \quad (13)$$

$$H_2PO_4^- + H^+ \rightleftharpoons H_3PO_4,\ pK_a = 2.12 \quad (14)$$

Nevertheless, a pH < 1.5 does not guarantee a complete P extraction since other extraction conditions (L/S ratio, acid concentration, and leaching time) could affect the leaching efficiency. The principal component analysis (PCA) was employed to determine the correlations between influential factors using OriginPro 2021 software. As shown in Fig. 4b, the first two principal components (PCs) retained 87% (accu-mulated) of explained variance. PC1 was positively contributed by eluate pH and leaching time, with correlation coefficients (r) of 0.64 and 0.54, respectively, but negatively contributed by acid concentration ($r = -0.54$). PC2 mainly depended on acid concentration ($r = 0.48$) and L/S ratio ($r = -0.82$) that contributed positively and negatively, respectively. The PCA results suggested that eluate pH was the most determinant variable that was positively related to leaching time and L/S ratio and negatively associated with acid concentration. A previous study also concluded similar findings for P extraction from ISSA (Luyckx et al., 2020). Consequently, while satisfying other factors, retaining an eluate pH < 1.5 could leach most P from hydrochar.

3.2.5. *Co-leaching of heavy metals*

Heavy metals are inevitably co-leached during acidic extraction of P from hydrochar. Targeting higher P leaching efficiency generally leads to more release of heavy metals due to more free acids. Fig. 5 shows the impacts of various parameters on heavy metal leaching. Using 0.1 N HNO_3 for 24 h, increasing L/S ratio from 5 to 100 mL dramatically enhanced the leaching efficiency of Zn, Pb, Cr, Ni, Cu, and Mo from <4% to 53%, 62%, 34%, 18%, 13%, and 12%, respectively (Fig. 5a). How-ever, when controlling the eluate pH at 2, the release of heavy metals exhibited no or limited increase regarding higher L/S ratio (Fig. 5b). Pb and Cr were the most susceptible to L/S ratio, while Zn and Ni remained nearly constant, and Cu and Mo showed slight increases. This indicated

Table 2
Share of each mechanism in leaching of P and metals from hydrochar in 100 mL/g of 0.1 and 0.6 N HNO_3.

Elements	Acid concentration (N)	τ_F (min)	τ_P (min)	τ_R (min)	R^2
P	0.1	18	146	0	0.9993
	0.6	0	18	0	0.9547
Alkaline earth metals (AEMs)	0.1	0	205	0	0.9994
	0.6	0	18	0	0.9740
Transition metals (TMs)	0.1	0	255	18	0.9993
	0.6	0	28	0	0.9246
Post-transition metals (PTMs)	0.1	0	974	0	0.9992
	0.6	0	104	0	0.9421

Table 3
P precipitation efficiency (PPE) and compositions of precipitates at various precipitation pH (24 h maturation).

Precipitates[a]	HAP-5	HAP-5.5	HAP-6	HAP-13
Final pH (@25 °C)	5	5.5	6	13
Ca:P in suspension	1.8	1.9	2	1.7
pH adjusting reagent	30 g/L Ca $(OH)_2$	30 g/L Ca $(OH)_2$	30 g/L Ca $(OH)_2$	2 M KOH
PPE (%)	99.84±0.12	99.91±0.02	99.98±0.00	99.94 ±0.00
Ca:P in precipitates	0.40±0.01	0.47±0.08	0.72±0.01	1.70 ±0.02
Fe:P in precipitates	0.80±0.02	0.78±0.00	0.78±0.02	0.68 ±0.02
Al:P in precipitates	0.16±0.00	0.16±0.00	0.17±0.01	0.05 ±0.00

[a] number follows HAP means precipitation pH.

that the leaching of Zn and Ni depended on eluate pH rather than L/S ratio, while the other heavy metals could be affected by both L/S ratio and eluate pH. At fixed L/S (10 mL/g) and time (24 h) (Fig. 5c), acid concentration had positive effects on the extraction of heavy metals, especially Pb, Zn, Cr, and Cu, whereas Ni and Mo showed slight changes, which might be more influenced to L/S ratio. Similar results were pre-viously reported on Cu, Pb, Zn, and Ni release from ISSA by nitric acid (Fang et al., 2018a). With 0.6 N HNO_3 at 10 mL/g, all assessed heavy metals reached the equilibrium status within 10 min although there were slight increases at longer leaching time (Fig. 5d). This was also observed by Luyckx et al. (2020) on most heavy metals leaching from ISSA. Overall, the leachability of heavy metals from hydrochar ranked as Zn > Pb > Cr > Ni > Cu > Mo. Among those metals, Mo was the least leachable possibly for its insoluble forms, such as $FeMoO_4$ and $Fe_2(MoO_4)_3$ (Nikolenko et al., 2018). However, the leaching efficiencies could vary depending on the mineral composition of hydrochar. Indeed, the results suggested that controlling leaching conditions, e.g., low L/S ratio, low acid concentration, and short time could reduce the co-extraction of heavy metals and associated concerns for the following utilization of P extract. To maintain a high P extraction efficiency, the optimum conditions for low leaching of heavy metals were 10 mL/g of 0.6 N HNO_3 for 2 h. Although alkaline leaching can avoid the co-dissolution of heavy metals, it restricts P leaching efficiency (up to 70%) from hydrochar (Liu et al., 2021b). For example, NaOH-extractable P in digested sludge-derived hydrochar (obtained at 260 °C) was 42% (Ovsyannikova et al., 2019), while using 10 mL 1 N NaOH per g hydrochar leached only 4% P from primary sludge-derived hydrochar (obtained at 350 °C) (Ovsyannikova et al., 2020). It seems that the performance of alkaline extraction is largely affected by the feedstock composition (likely the amount of Al or Fe salts). Instead, acidic leaching could be a more reliable approach for efficient P re-covery from hydrochar.

3.3. Leaching kinetics

The shrinking core model was applied to the leaching process in 0.1 and 0.6 N HNO_3 at an L/S of 100 mL/g. Assuming only one rate-limiting step, the leaching rate versus time at each acid concentration was fitted to Eqs. (1)–(3) individually (Fig. 6). Based on the R^2 (>0.99), Eq. (2) showed the best correlation to the leaching of P and all metal groups for both 0.1 and 0.6 N HNO_3. This indicated that the leaching reaction rate was limited by product layer diffusion. The particle size distribution also suggested that the assumption of constant particle size was fulfilled (Fig. S2).

To validate the single-controlling mechanism, leaching data were tested by the combined resistances method expressed by Eqs. (4)–(5), and share (τ_F, τ_P, and τ_R) of each step was calculated in Table 2. The results suggested that product layer diffusion had the most share in leaching rates, although liquid film diffusion and chemical reaction contributed marginally to the P and TMs leaching, respectively, in 0.1 N HNO_3. The resistance from liquid film might be caused by the small particle size, while the chemical reaction could be between iron oxides and acid (Nazemi et al., 2011; H.H. Wang et al., 2017). The leaching data at 0.6 N generally showed a poorer correlation (lower R^2) than those at 0.1 N, which was attributed to the convection at a high eluent concentration (Liddell, 2005). Remarkably, the higher acid normality (0.6 N) significantly cut the completion time of the leaching process nearly ten times, demonstrating that excessive amounts of acid could be used to reduce the retention time in industrial applications. Based on the estimated completion time, the diffusion rate could be ranked as P > AEMs > TMs > PTMs.

Both the better correlation of linear fitting and the higher share in the leaching rate confirmed that product layer diffusion was the governing rate-limiting step for P and metals leaching from hydrochar in nitric acid. The same mechanism was reported for P leaching from phosphate rock by H_2SO_4 (Liu et al., 2021), dephosphorization slag by HCl (Du et al., 2020), and rice husk ash by HCl (J. Wang et al., 2017). The diffusion mechanism suggests that the leaching process is sensitive to agitation and particle size but insensitive to temperature (Faraji et al., 2020). Intensive stirring (1200 rpm) could achieve > 90% of P extraction efficiency within 10 min from ISSA (Franz, 2008). According to the

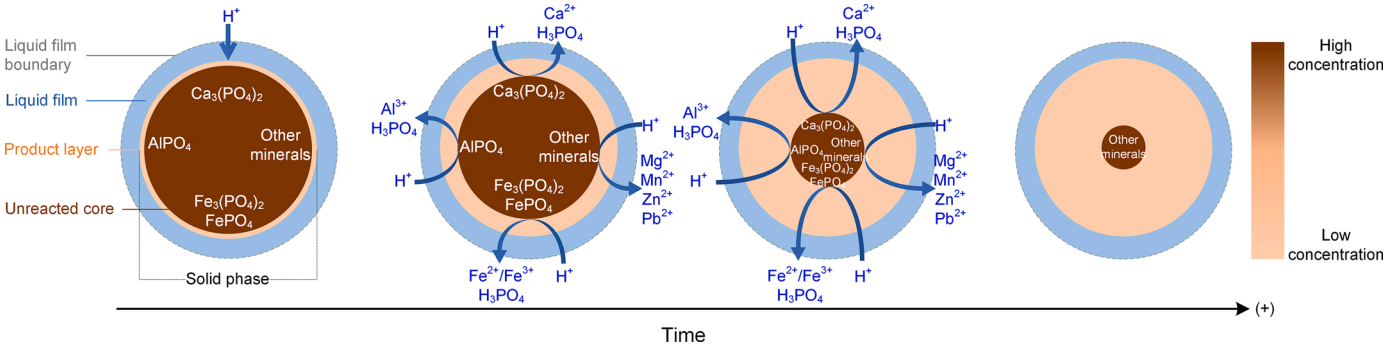

Fig. 7. Leaching process of P and metals from hydrochar particles by excessive acid (e.g., 100 mL/g of 0.1 N HNO_3).

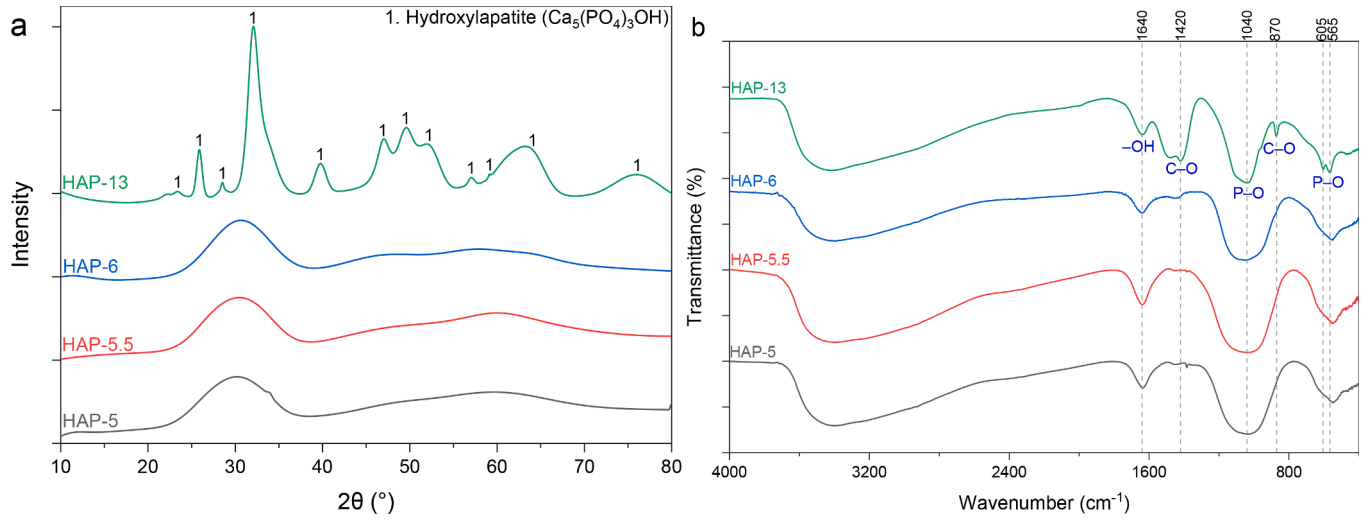

Fig. 8. (a) XRD patterns and (b) FTIR spectra of recovered precipitates.

shrinking core model, the leaching process can be described as follows (Fig. 7): (1) In a short period, acid (H^+) diffuses from solution through the liquid film around hydrochar particles; (2) acid quickly reacts with minerals to release phosphates and metals; (3) soluble reaction products gradually diffuses through the product layer and quickly diffuses through the liquid film to the solution; (4) reaction continues until reaching the particle center. Finding the controlling mechanism of P leaching from hydrochar is reported for the first time in the literature by this study, which has a significant contribution to designing an efficient P recovery process.

3.4. P recovery by precipitation

After extraction using 10 mL/g of 0.6 N HNO_3 for 2 h, phosphate was precipitated by adjusting pH and Ca:P molar ratio to generate hy-droxyapatite (HAP). To achieve a near-neutral pH for precipitation, Ca $(OH)_2$ was dosed at slightly higher Ca:P molar ratios (1.7–2) than the theoretical value (1.67) in hydroxyapatite. As shown in Table 3, the PPE could reach >99% with only slight increases when pH increased from 5 to 6, in agreement with the literature (Liu et al., 2021b). However, the actual Ca:P (0.40–0.72) in precipitates (HAP-5 and HAP-6) were far below the target molar ratio, indicating the failure of HAP synthesis. The reason was mainly due to the competition from iron (Fe:$P > 0.78$) and the co-precipitation of $FePO_4$ (Yan and Shih, 2016). The XRD and FTIR results also did not observe hydroxyapatite or crystalline phosphates in precipitates obtained at pH 5–6 (Fig. 8). Previous studies suggested that foreign metal ions (particularly Zn^{2+}) could inhibit the crystallization of phosphate minerals and also attach to crystal surface and interfere XRD patterns (Dai et al., 2018). Considering most foreign metal ions are amphoteric and their forms strongly depend on pH, chemical equilib-rium modeling as a function of precipitation pH was performed by Vi-sual MINTEQ 3.1 software (Fig. S3). The results indicate that the saturation index (SI) of HAP is positive at pH > 4 and increases at higher pH until reaches the maximum at pH > 9. The SI values of foreign minerals (e.g., strengite and $Zn_3(PO_4)_2$) also enhance with increasing pH but then mostly decrease to below 0 at pH > 12. Therefore, a high pH may mitigate the effects of foreign ions and improve crystallization.

Enhancing the pH to 13 by adding KOH solution, all P precipitated at a Ca:P of 1.7 (Table 3). Notably, the actual Ca:P in the recovered HAP-13 achieved the target Ca:P, with the decrease of Fe:P and Al:P. Both XRD and FTIR spectra proved the formation of crystal phosphates (hy-droxyapatite). Compared to broad peaks ($2\theta = 30°$) of amorphous P in

Table 4
P and metal contents (dry basis) in recovered precipitates compared to Canadian fertilizer regulation.

Concentration	Precipitates[a]				Max acceptable concentration (mg/kg) based on annual application rate[b]		
	HAP-5	HAP-5.5	HAP-6	HAP-13	4400 kg/ha	2000 kg/ha	500 kg/ha
P (%)	18.6 ± 0.4	18.9 ± 0.7	16.3 ± 0.5	11.3 ± 0.9			
P_2O_5 (%)	43±1	43±2	37±1	26±2			
Available P_2O_5 (%)[b]	26±0	34±2	37±2	25±0			
Ca (%)	9.73±0.02	11.4 ± 2.3	15.1 ± 0.2	24.9 ± 1.7			
Mg (%)	0.11±0.01	0.18±0.06	0.34±0.00	0.96±0.01			
Fe (%)	26.8 ± 1.3	26.6 ± 0.8	22.9 ± 0.1	13.9 ± 0.7			
Al (%)	2.52±0.08	2.59±0.03	2.48±0.00	0.53±0.01			
K (mg/kg)	1793±135	1841±793	1248±34	857±41			
Na (mg/kg)	262±116	234±121	312±6	135±7			
Cr (mg/kg)	196±2	195±5	198±3	109±3	1060	2333	9333
Cu (mg/kg)	209±8	226±8	203±3	463±189	757	1666	6666
Mn (mg/kg)	1615±171	1906±41	2310±64	1218±7			
Mo (mg/kg)	5.35±0.03	5.5 ± 0.4	5.3 ± 0.6	1.3 ± 0.6	20	44	177
Ni (mg/kg)	17.5 ± 0.3	25±2	36±4	23±3	181	400	1600
Zn (mg/kg)	3706±89	3813±58	3575±117	2669±232	1868	4111	16,444
Pb (mg/kg)	214±24	192±16	195±8	126±10	505	1111	4444
P availability (% of toal)[c]	61±1	78±3	100±3	95±6			

[a] number follows HAP means precipitation pH.
[b] Canadian Food Inspection Agency (CFIA), *T-4–93 – Safety standards for fertilizers and supplements* (as of October 26, 2020).
[c] Extractable by 2% citric acid.

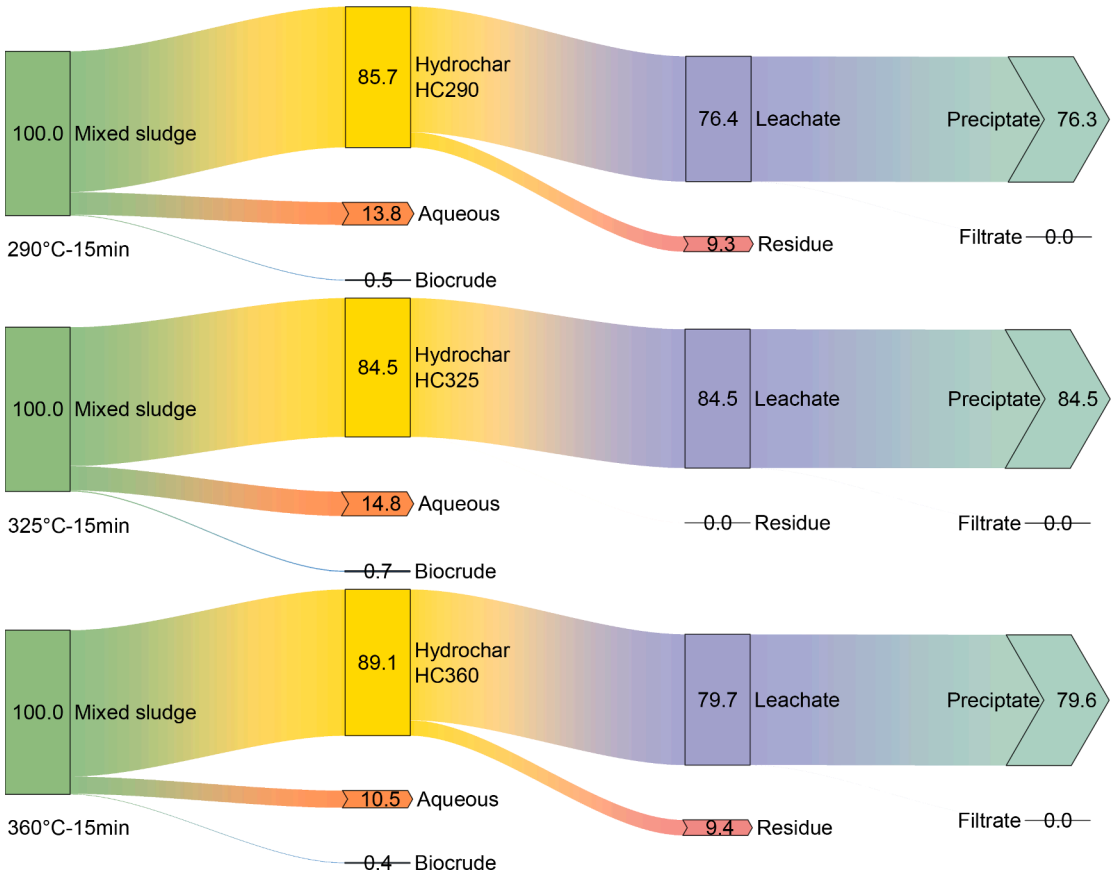

Fig. 9. P flow (%) diagram at various HTL reaction temperatures (15 min residence time) based on sludge input, integrating P extraction (L/S = 10 mL/g, 0.6 N HNO_3, 2 h) and precipitation (Ca/P = 1.7, pH=13, 24 h) from hydrochar.

other precipitates, HAP-13 showed numerous sharp peaks corresponding to hydroxyapatite in XRD (Fig. 8a). The FTIR spectra (Fig. 8b) only identified hydroxyl groups (1640 cm^{-1}) and board band (1200–900 cm^{-1}) of amorphous phosphates in precipitates obtained at pH 5–6, while HAP-13 displayed several peaks (1040, 605, and 565 cm^{-1}) of crystal phosphates with some carbonate groups (1420 and 870 cm^{-1}) (Pham Minh et al., 2014). Petzet et al. (2012) also synthesized hydroxyapatite from NaOH-extracted sludge ash, and the strategy was converting Al-P into Ca-P at pH 13. The results demonstrated that a pH ≥ 5 could precipitate almost all P in extracts from hydrochar, whereas a higher pH (e.g., 13) would be necessary to produce hydroxyapatite.

3.5. Recovered precipitates as fertilizers

Precipitation of P from acid extracts by $Ca(OH)_2$ is efficient at both neutral (5–6) and high pH (13). However, the recovered precipitates have different compositions that will affect their usage. As presented in Table 4, all the recovered precipitates had high concentrations of P comparable to calcium phosphate fertilizers (e.g., superphosphates). Notably, the pH increase decreased P_2O_5 content from 43% in HAP-5 to 26% in HAP-13. This change could be related to the increase of "basic" species, e.g., HPO_4^{2-} and PO_4^{3-}, that bind more metal cations (Liu et al., 2018). Conversely, the plant availability of P increased from 61% to 100%. It was suggested that aluminum and iron phosphates generally have limited available P, while their conversion into Ca-P by additional $Ca(OH)_2$ or pH enhancement could improve P availability (Fang et al., 2018b). Although the multifunctional hydroxyapatite could be synthesized at a pH of 13, there is a compromise of additional chemicals for pH adjustment. Therefore, process optimization would be useful to make it more economical. Overall, the recovered precipitates showed good amounts of available P as fertilizers, with the potential for broader application.

As hydrochar is often concentrated with heavy metals that could be leached by acids, the presence of contaminants in recovered products is concerning for agricultural use. Although the chemical equilibrium modeling (Fig. S3) suggested that most heavy metals should exist in soluble forms at pH 13, their actual concentrations in HAP-13 were high (Table 4). This was attributed to the strong adsorption capacity of hy-droxyapatite (Pham Minh et al., 2014). The total heavy metals in recovered precipitates generally followed the order of Zn > Cu > Pb > Cr > Ni > Mo, consistent with those in the original hydrochar. The total Pb and Zn in precipitates are relatively higher than those recovered from sewage sludge ash, which also exceeds the fertilizer criteria in the EU (Liu et al., 2021b). In Canada and the US, standards for heavy metals in fertilizers are risk-based, which depend on the annual application rate and percentage of P in fertilizers, respectively (Table S2). According to Canadian regulation (Table 4), the heavy metals contents in recovered precipitates are well below the criteria if the fertilizer application rate maintains under 2000 kg/ha per year (far beyond the regular applica-tion rate, <80 kg/ha, in Canada) (Wang et al., 2022). Their concentra-tions are also acceptable based on the US limits after multiplying the%P_2O_5. Nevertheless, metals in hydrochar can co-leach and co-precipitate during the recovery process and affect the quality of recovered products, and thus purification steps should be considered.

3.6. Application of recovery process to different hydrochar

Applying the optimal extraction (0.6 N HNO_3 at L/S = 10 mL/g for 2 h) and precipitation (Ca:*P* = 1.7 at pH 13 for 24 h) conditions to other hydrochar samples, the overall P flow at various hydrothermal condi-tions is illustrated in Fig. 9. The P distribution at different HTL reaction temperatures (290–360 °C) has been reported previously (Liu et al.,

2023). Overall, around 85% of P was captured in hydrochar (HC290 and HC325) from mixed sludge at 290 and 325 °C, while a slightly higher recovery (89%) was obtained at 360 °C (HC360). The highest P extraction efficiency (nearly 100%) was achieved for hydrochar from medium HTL temperature (325 °C) (Fig. S4). P leaching from HC290 and HC360 was also satisfactory despite a lower leaching rate (89%). Compared to extraction, the performance of precipitation step seems to be more stable. Almost all P in solutions from different hydrochar could be precipitated (Table S3), with the successful synthesis of hydroxyap-atite (Fig. S5). The recovered precipitates also had acceptable contents of plant-available P and heavy metals in Canada and the US. In sum-mary, considering the holistic process, the total P recovery efficiency was between 76 and 85% based on the sludge input. The hydrothermal temperature is influential on the P distribution and extraction efficiency, and HTL at 325 °C for 15 min was found as the best scenario. Most P losses occurred during the hydrothermal treatment and extraction step that require additional investigations to enhance the overall recovery.

4. Conclusion

Recovering P from hydrochar is promising and favorable for promoting the integration of HTL into WWTPs. This study demonstrated the performance of a simple and reproducible P recovery process. The following conclusions are drawn:

- Nitric acid is efficient for P extraction. All assessed variables showed significant impacts on P and metals leaching efficiencies. Higher L/S ratios (e.g., 100 mL/g) improved extraction but consumed more acid. A leaching time of 2 h was sufficient to achieve chemical equilibrium but can be shortened by higher acid concentration. The eluate pH was a dominant factor controlling P leaching, related to the interactions with Fe and Al. The optimal extraction conditions balancing the leaching of P and heavy metals were 10 mL/g of 0.6 N HNO_3 for 2 h. However, the conditions should be further tested and optimized for other HTL feedstock types as the extraction conditions can vary depending on P and metal contents as well as mineral species. For future optimization studies, the eluate pH can be used as a monitoring factor.
- The kinetic analysis suggested that the leaching of P and metals from hydrochar was limited by product layer diffusion, meaning that the leaching process is sensitive to stirring and particle size but not temperature. The diffusion rate was ranked as P > AEMs > TMs > PTMs.
- The addition of $Ca(OH)_2$ to P extracts could precipitate most P at a pH of 5–6 but not form hydroxyapatite due to the interference of co-leached metals (e.g., Zn). Enhancing pH to 13 successfully produced hydroxyapatite. The recovered precipitates had acceptable values of plant-available P and total heavy metals in Canada and the US for land application. However, the precipitation step requires optimization for reducing costs and improving product quality.
- The developed P recovery procedures were applicable to hydrochar from various HTL conditions. However, the P capture in hydrochar and its extraction from hydrochar were affected by HTL reaction temperatures that require further investigation. Overall, HTL at 325 °C for 15 min could be the best process operation for energy and P recovery from municipal sludge and its hydrochar.

Declaration of Competing Interest

The authors declare that they have no known competing financial interests or personal relationships that could have appeared to influence the work reported in this paper.

Data availability

Data will be made available on request.

Acknowledgments

This work was funded by Natural Sciences and Engineering Research Council of Canada (NSERC) and Metro Vancouver Industrial Research Chair Program (IRCPJ 548816–18) in Advanced Resource Recovery from Wastewater; and NSERC Canada Graduate Scholarship – Doctoral program. The improvements contributed by the Editor and anonymous reviewers are acknowledged.

References

Agbeboh, N.I., Oladele, I.O., Daramola, O.O., Adediran, A.A., Olasukanmi, O.O., Tanimola, M.O., 2020. Environmentally sustainable processes for the synthesis of hydroxyapatite. Heliyon 6, e03765. https://doi.org/10.1016/j.heliyon.2020.e03765.

Arokiasamy, P., Al Bakri Abdullah, M.M., Abd Rahim, S.Z., Luhar, S., Sandu, A.V., Jamil, N.H., Nabiałek, M., 2022. Synthesis methods of hydroxyapatite from natural sources: A review. Ceram. Int. 48, 14959–14979. https://doi.org/10.1016/j.ceramint.2022.03.064.

Banihashemi, S.R., Taheri, B., Razavian, S.M., Soltani, F., 2019. Selective Nitric Acid Leaching of Rare-Earth Elements from Calcium and Phosphate in Fluorapatite Concentrate. JOM 71, 4578–4587. https://doi.org/10.1007/s11837-019-03605-6.

Basar, I.A., Liu, H., Carrere, H., Trably, E., Eskicioglu, C., 2021. A review on key design and operational parameters to optimize and develop hydrothermal liquefaction of biomass for biorefinery applications. Green Chem. 23, 1404–1446. https://doi.org/10.1039/D0GC04092D.

Basar, I.A., Liu, H., Eskicioglu, C., 2023. Incorporating hydrothermal liquefaction into wastewater treatment – Part III: Aqueous phase characterization and evaluation of on-site treatment. Chem. Eng. J. 467, 143422 https://doi.org/10.1016/j.cej.2023.143422.

Becker, G.C., Wüst, D., Köhler, H., Lautenbach, A., Kruse, A., 2019. Novel approach of phosphate-reclamation as struvite from sewage sludge by utilising hydrothermal carbonization. J. Environ. Manage. 238, 119–125. https://doi.org/10.1016/j.jenvman.2019.02.121.

Dai, H., Tan, X., Zhu, H., Sun, T., Wang, X., 2018. Effects of commonly occurring metal ions on hydroxyapatite crystallization for phosphorus recovery from wastewater. Water (Switzerland) 10, 1619. https://doi.org/10.3390/w10111619.

Du, C.ming, Gao, X., Ueda, S., Kitamura, S.ya, 2020. A Kinetic Study on Selective Leaching of Phosphorus from Dephosphorization Slag. J. Sustain. Metall. 6, 724–738. https://doi.org/10.1007/s40831-020-00309-z.

Fahimi, A., Federici, S., Depero, L.E., Valentim, B., Vassura, I., Ceruti, F., Cutaia, L., Bontempi, E., 2021. Evaluation of the sustainability of technologies to recover phosphorus from sewage sludge ash based on embodied energy and CO2 footprint. J. Clean. Prod. 289, 125762 https://doi.org/10.1016/j.jclepro.2020.125762.

Fang, L., Li, J., Guo, M.Z., Cheeseman, C.R., Tsang, D.C.W., Donatello, S., Poon, C.S., 2018a. Phosphorus recovery and leaching of trace elements from incinerated sewage sludge ash (ISSA). Chemosphere 193, 278–287. https://doi.org/10.1016/j.chemosphere.2017.11.023.

Fang, L., Li, J.shan, Donatello, S., Cheeseman, C.R., Wang, Q., Poon, C.S., Tsang, D.C.W., 2018b. Recovery of phosphorus from incinerated sewage sludge ash by combined two-step extraction and selective precipitation. Chem. Eng. J. 348, 74–83. https://doi.org/10.1016/j.cej.2018.04.201.

Faraji, F., Alizadeh, A., Rashchi, F., Mostoufi, N., 2020. Kinetics of leaching: A review. Rev. Chem. Eng. https://doi.org/10.1515/revce-2019-0073.

Franz, M., 2008. Phosphate fertilizer from sewage sludge ash (SSA). Waste Manag. 28, 1809–1818. https://doi.org/10.1016/j.wasman.2007.08.011.

He, P., Zhang, X., Lü, F., Shao, L., Zhang, H., 2020. Leaching behavior of phosphorous compounds from sewage sludge ash based on quantitative X-ray diffraction analysis. Waste Dispos. Sustain. Energy 2, 113–125. https://doi.org/10.1007/s42768-020-00037-w.

Huang, R., Fang, C., Lu, X., Jiang, R., Tang, Y., 2017. Transformation of phosphorus during (hydro)thermal treatments of solid Biowastes: Reaction mechanisms and implications for P reclamation and recycling. Environ. Sci. Technol. 51, 10284–10298. https://doi.org/10.1021/acs.est.7b02011.

Li, S., Zeng, W., Jia, Z., Wu, G., Xu, H., Peng, Y., 2020. Phosphorus species transformation and recovery without apatite in FeCl3-assisted sewage sludge hydrothermal treatment. Chem. Eng. J. 399, 125735 https://doi.org/10.1016/j.cej.2020.125735.

Liddell, K.C., 2005. Shrinking core models in hydrometallurgy: What students are not being told about the pseudo-steady approximation. Hydrometallurgy 79, 62–68. https://doi.org/10.1016/j.hydromet.2003.07.011.

Liu, H., Basar, I.A., Lyczko, N., Nzihou, A., Eskicioglu, C., 2022. Incorporating hydrothermal liquefaction into wastewater treatment – Part I: Process optimization for energy recovery and evaluation of product distribution. Chem. Eng. J. 449, 137838 https://doi.org/10.1016/j.cej.2022.137838.

Liu, H., Basar, I.A., Nzihou, A., Eskicioglu, C., 2021a. Hydrochar derived from municipal sludge through hydrothermal processing: A critical review on its formation, characterization, and valorization. Water Res. 199, 117186 https://doi.org/10.1016/j.watres.2021.117186.

Liu, H., Hu, G., Basar, I.A., Li, J., Lyczko, N., Nzihou, A., Eskicioglu, C., 2021b. Phosphorus recovery from municipal sludge-derived ash and hydrochar through wet-chemical technology: A review towards sustainable waste management. Chem. Eng. J. 417, 129300 https://doi.org/10.1016/j.cej.2021.129300.

Liu, H., Lyczko, N., Nzihou, A., Eskicioglu, C., 2023. Incorporating hydrothermal liquefaction into wastewater treatment – Part II: Characterization, environmental impacts, and potential applications of hydrochar. J. Clean. Prod. 383, 135398 https://doi.org/10.1016/j.jclepro.2022.135398.

Liu, J., Cheng, X., Qi, X., Li, N., Tian, J., Qiu, B., Xu, K., Qu, D., 2018. Recovery of phosphate from aqueous solutions via vivianite crystallization: Thermodynamics and influence of pH. Chem. Eng. J. 349, 37–46. https://doi.org/10.1016/j.cej.2018.05.064.

Liu, R., Long, Y., Zhou, Y., Liu, Z., Liu, X., Huo, X., Xie, Z., Tao, C., 2021. Rigid-Flexible Combined Impeller Enhancement in Leaching of Phosphate Rock: A Kinetics Study. ACS Omega 6, 33206–33214. https://doi.org/10.1021/acsomega.1c05836.

Luyckx, L., Geerts, S., Van Caneghem, J., 2020. Closing the phosphorus cycle: Multi-criteria techno-economic optimization of phosphorus extraction from wastewater treatment sludge ash. Sci. Total Environ. 713, 135543 https://doi.org/10.1016/j.scitotenv.2019.135543.

Marin-Batista, J.D., Mohedano, A.F., Rodríguez, J.J., de la Rubia, M.A., 2020. Energy and phosphorous recovery through hydrothermal carbonization of digested sewage sludge. Waste Manag. 105, 566–574. https://doi.org/10.1016/j.wasman.2020.03.004.

Marrone, P.A., Elliott, D.C., Billing, J.M., Hallen, R.T., Hart, T.R., Kadota, P., Moeller, J.C., Randel, M.A., Schmidt, A.J., 2018. Bench-scale evaluation of hydrothermal processing technology for conversion of wastewater solids to fuels. Water Environ. Res. 90, 329–342. https://doi.org/10.2175/106143017x15131012152861.

Nazemi, M.K., Rashchi, F., Mostoufi, N., 2011. A new approach for identifying the rate controlling step applied to the leaching of nickel from spent catalyst. Int. J. Miner. Process. 100, 21–26. https://doi.org/10.1016/j.minpro.2011.04.006.

Nikolenko, N.V., Kozhevnikov, I.V., Kostyniuk, A.O., Bayahia, H., Kalashnykov, Y.V., 2018. Preparation of iron molybdate catalysts for methanol to formaldehyde oxidation based on ammonium molybdoferrate(II) precursor. J. Saudi Chem. Soc. 22, 372–379. https://doi.org/10.1016/j.jscs.2016.04.002.

Ottosen, L.M., Kirkelund, G.M., Jensen, P.E., 2013. Extracting phosphorous from incinerated sewage sludge ash rich in iron or aluminum. Chemosphere 91, 963–969. https://doi.org/10.1016/j.chemosphere.2013.01.101.

Ovsyannikova, E., Arauzo, P.J., Becker, G., Kruse, A., 2019. Experimental and thermodynamic studies of phosphate behavior during the hydrothermal carbonization of sewage sludge. Sci. Total Environ. 692, 147–156. https://doi.org/10.1016/j.scitotenv.2019.07.217.

Ovsyannikova, E., Kruse, A., Becker, G.C., 2020. Feedstock-Dependent Phosphate Recovery in a Pilot-Scale Hydrothermal Liquefaction Bio-Crude Production. Energies 13, 379. https://doi.org/10.3390/en13020379.

Pérez, C., Boily, J.F., Jansson, S., Gustafsson, T., Fick, J., 2021. Acid-Induced Phosphorus Release from Hydrothermally Carbonized Sewage Sludge. Waste Biomass Valoriz. 12, 6555–6568. https://doi.org/10.1007/s12649-021-01463-5.

Pérez, C., Boily, J.F., Skoglund, N., Jansson, S., Fick, J., 2022. Phosphorus release from hydrothermally carbonized digested sewage sludge using organic acids. Waste Manag. 151, 60–69. https://doi.org/10.1016/j.wasman.2022.07.023.

Petzet, S., Peplinski, B., Cornel, P., 2012. On wet chemical phosphorus recovery from sewage sludge ash by acidic or alkaline leaching and an optimized combination of both. Water Res. 46, 3769–3780. https://doi.org/10.1016/j.watres.2012.03.068.

Pham Minh, D., Rio, S., Sharrock, P., Sebei, H., Lyczko, N., Tran, N.D., Raii, M., Nzihou, A., 2014. Hydroxyapatite starting from calcium carbonate and orthophosphoric acid: Synthesis, characterization, and applications. J. Mater. Sci. 49, 4261–4269. https://doi.org/10.1007/s10853-014-8121-7.

Rego de Vasconcelos, B., Pham Minh, D., Sharrock, P., Nzihou, A., 2018. Regeneration study of Ni/hydroxyapatite spent catalyst from dry reforming. Catal. Today 310, 107–115. https://doi.org/10.1016/j.cattod.2017.05.092.

Shi, Y., Luo, G., Rao, Y., Chen, H., Zhang, S., 2019. Hydrothermal conversion of dewatered sewage sludge: Focusing on the transformation mechanism and recovery of phosphorus. Chemosphere 228, 619–628. https://doi.org/10.1016/j.chemosphere.2019.04.109.

Soltani, F., Abdollahy, M., Petersen, J., Ram, R., Javad Koleini, S.M., Moradkhani, D., 2019. Leaching and recovery of phosphate and rare earth elements from an iron-rich fluorapatite concentrate: Part II: Selective leaching of calcium and phosphate and acid baking of the residue. Hydrometallurgy 184, 29–38. https://doi.org/10.1016/j. hydromet.2018.12.024.

Toor, U.A., Kim, D.J., 2019. Effect of pH on phosphorus (P) dissolution and recovery from polyaluminum chlorides (PAC) sludge. J. Environ. Manage. 239, 142–149. https://doi.org/10.1016/j.jenvman.2019.03.049.

Verwilghen, C., Rio, S., Nzihou, A., Gauthier, D., Flamant, G., Sharrock, P.J., 2007. Preparation of high specific surface area hydroxyapatite for environmental applications. J. Mater. Sci. 42, 6062–6066. https://doi.org/10.1007/s10853-006-1160-y.

Wang, H.H., Li, G.Q., Zhao, D., Ma, J.H., Yang, J., 2017. Dephosphorization of high phosphorus oolitic hematite by acid leaching and the leaching kinetics. Hydrometallurgy 171, 61–68. https://doi.org/10.1016/j.hydromet.2017.04.015. Wang, J., Qi, Z., Bennett, E.M., 2022. Changes in Canada's Phosphorus Cycle 1961–2018: Surpluses and Deficits. Glob. Biogeochem. Cycles 36. https://doi.org/10.1029/2022GB007407.

Wang, J., Zhuang, X., Kong, J., Liu, Y., Du, X., Luo, X., Xing, P., 2017. Kinetics analysis of leaching phosphorus from rice husk ash assisted by ultrasound. Sep. Sci. Technol. 52, 1265–1274. https://doi.org/10.1080/01496395.2017.1287198.

Wang, Q., Zhang, C., Liu, P., Jung, H., Wan, B., Patel, D., Pavlostathis, S.G., Tang, Y., 2020. Effect of Interstage Hydrothermal Treatment on Anaerobic Digestion of Sewage Sludge: Speciation Evolution of Phosphorus, Iron, and Sulfur. ACS Sustain. Chem. Eng. 8, 16515–16525. https://doi.org/10.1021/acssuschemeng.0c05544.

Yan, H., Shih, K., 2016. Effects of calcium and ferric ions on struvite precipitation: A new assessment based on quantitative X-ray diffraction analysis. Water Res. 95, 310–318. https://doi.org/10.1016/j.watres.2016.03.032.